Haloalkane Dehalogenases: Structure of a *Rhodococcus* Enzyme[†,‡]

Janet Newman,*[,§,||] Thomas S. Peat,[§,||] Ruth Richard,[⊥] Lynn Kan,[⊥] Paul E. Swanson,[⊥] Joseph A. Affholter,[⊥,○] Ian H. Holmes,[#] John F. Schindler,[⊗] Clifford J. Unkefer,*[,⊗] and Thomas C. Terwilliger*[,§]

Life Sciences Division, Theory Division, and Chemical Science and Technology Division, Los Alamos National Laboratory, Los Alamos, New Mexico 87545, and The Dow Chemical Company, 1707 Building, Midland, Michigan 48674

Received June 16, 1999; Revised Manuscript Received September 24, 1999

ABSTRACT: The hydrolytic haloalkane dehalogenases are promising bioremediation and biocatalytic agents. Two general classes of dehalogenases have been reported from *Xanthobacter* and *Rhodococcus*. While these enzymes share 30% amino acid sequence identity, they have significantly different substrate specificities and halide-binding properties. We report the 1.5 Å resolution crystal structure of the *Rhodococcus* dehalogenase at pH 5.5, pH 7.0, and pH 5.5 in the presence of NaI. The *Rhodococcus* and *Xanthobacter* enzymes have significant structural homology in the α/β hydrolase core, but differ considerably in the cap domain. Consistent with its broad specificity for primary, secondary, and cyclic haloalkanes, the *Rhodococcus* enzyme has a substantially larger active site cavity. Significantly, the *Rhodococcus* dehalogenase has a different catalytic triad topology than the *Xanthobacter* enzyme. In the *Xanthobacter* dehalogenase, the third carboxylate functionality in the triad is provided by D260, which is positioned on the loop between β7 and the penultimate helix. The carboxylate functionality in the *Rhodococcus* catalytic triad is donated from E141. A model of the enzyme cocrystallized with sodium iodide shows two iodide binding sites; one that defines the normal substrate and product-binding site and a second within the active site region. In the substrate and product complexes, the halogen binds to the *Xanthobacter* enzyme via hydrogen bonds with the $N^{\eta}H$ of both W125 and W175. The *Rhodococcus* enzyme does not have a tryptophan analogous to W175. Instead, bound halide is stabilized with hydrogen bonds to the $N^{\eta}H$ of W118 and to $N^{\delta}H$ of N52. It appears that when cocrystallized with NaI the *Rhodococcus* enzyme has a rare stable S−I covalent bond to S^{γ} of C187.

The haloalkane dehalogenases catalyze the irreversible hydrolysis of a variety of haloalkanes to the corresponding alcohol, halide, and a hydrogen ion (*1*−*4*). On the basis of sequence analysis, two general classes of hydrolytic haloalkane dehalogenases have been identified and can be represented by the enzymes from *Xanthobacter autotrophicus* GJ10 (*Xa*DHL[1]) and *Rhodococcus rhodochrous* (*Rr*DHL[1]) (*5*). Historical interest in these enzymes stems from their potential use in remediation of sites contaminated with halogenated solvents (*6*−*8*). In addition to haloalkanes' widespread application as solvents, they are generated as side products of industrial chemical processes. For example, the production of commodity epoxides through halohydrin chemistry yields several 1,2-dichloroalkanes as side products. Traditional chemical approaches have not yielded economically viable processes to convert these side products into higher value chemicals. Our interest in haloalkane dehalogenases stems from their potential application in recovery of these industrial side products. Potential dehalogenase substrates 1,2-dichloropropane, 1,2,3-trichloropropane, and 1,2-dichlorobutane are of particular interest, because their corresponding halohydrins can be used as starting materials for the commercial epoxide production. Because *Xa*DHL is a poor catalyst for these industrially useful substrates (*4*), we embarked on a screening program, which identified a number *Rhodococcus* species capable of growth on chloroalkanes as their sole source of carbon. We selected for further development a *Rhodococcus* dehalogenase that had higher activity toward multiply halogenated, and longer chain (>C4) alkanes. This enzyme is similar in sequence to the dehalo-

* Correspondence addressed to: C. J. Unkefer, Los Alamos National Laboratory, M. S. G758, Los Alamos, NM 87545. E-mail: cju@lanl.gov. J. Newman, Structural GenomiX, 10505 Roselle St., San Diego, CA 92121. E-mail: janet@stromix.com. T. C. Terwilliger, Los Alamos National Laboratory, M. S. M888, Los Alamos, NM 87545. E-mail: terwilliger@lanl.gov.

† This research supported by grants from The Dow Chemical Company and the National Institutes of Health and was performed under the auspices of the Laboratory Directed Research and Development Program at Los Alamos National Laboratory. Los Alamos National Laboratory is operated by the University of California for the U. S. Department of Energy under Contract W-7405-ENG-36.

‡ The coordinates have been deposited with the Protein Data Base, and have accession numbers: 1bn7 (pH 5.5 coordinates, data), 1bn6 (pH 7.0 coordinates, data), 1cqw (NaI complex coordinates).

§ Life Sciences Division, Structural Biology Group.

|| Present address: Structural GenomiX, 10505 Roselle St., San Diego, California 92121.

⊥ The Dow Chemical Company.

○ Present address: Maxygen, Inc., 3410 Central Expressway, Santa Clara, California 95051.

Theory Division, Theoretical Biology Group.

⊗ Chemical Science and Technology Division, Bioscience and Biotechnology Group.

[1] Abbreviations: *Xa*DHL, haloalkane dehalogenase from *Xanthobacter autotrophicus* GJ10; *Rr*DHL, haloalkane dehalogenase from *Rhodococcus rhodochrous*; PCR, polymerase chain reaction; PEG, poly(ethylene glycol); NSLS, BNL, National Synchrotron Light Source, Brookhaven National Laboratory; MIR multiple isomorphous replacement; rmsd, root-mean-square deviation.

10.1021/bi9913855 CCC: $18.00
Published on Web 11/12/1999

genase from *Rhodococcus rhodochrous*, which is also known to have broader substrate specificity then the *Xa*DHL (*4*). To date, no structural data has been presented on the *Rhodococcus* dehalogenases.

The structure of the *Xanthobacter* dehalogenase has been characterized in the laboratories of Janssen and Dijkstra (*9*−*14*). *Xa*DHL falls into a superfamily of protease-like proteins, which adopt the α/β hydrolase fold consisting of eight strands of β-sheet connected by α-helices (*15, 16*). An excursion from the hydrolase core of *Xa*DHL forms a cap domain, which is not conserved through out the superfamily. In addition to the overall fold, the α/β hydrolase superfamily preserved the arrangement of a triad of catalytic residues represented by a nucleophilic residue (Cys, Asp, or Ser) a conserved histidine, and an acidic residue (Asp or Glu). In *Xa*DHL, this triad of residues is represented by D124, H289, and D260, respectively (*9, 10*). X-ray crystal analysis (*9, 10*) and site-directed mutations (*11, 12*) have demonstrated that these residues are involved in the dehalogenation mechanism. After formation of the Michaelis complex, the side chain carboxylate of the nucleophilic aspartate (D124) displaces a halide ion from the substrate, forming a covalent ester intermediate. Next, the intermediate ester is saponified by hydroxide produced from a water molecule at the active site by H289. The imidazole side chain of H289 is present in the HN^{δ} tautomeric form and is activated by a hydrogen bond through its N^{δ} proton to the carboxylate of D260. The imidazole N^{ϵ} of H289 acts as a general base abstracting a proton from the active site water, and the resulting hydroxide ion attacks the C^{γ} of the D124 ester intermediate.

Two tryptophan residues, W125 and W175, are involved in substrate and product binding by *Xa*DHL. Crystal structures of *Xa*DHL obtained under acidic conditions (pH 5.2) and in the presence of chloride or iodide indicate that halide ion binds the enzyme by interactions with two indole side chains of W125 and W175. The bound halide is located at equal distance from the N^{η} of W125 (3.4 Å) and N^{η} of W175 (3.3 Å) (*10*). A structure obtained at low pH (pH 5.2), low temperature (4 °C), and in the presence of 1,2-dichloroethane shows substrate bound to *Xa*DHL in the *trans*-configuration and with the leaving halide positioned between the indole NH's of W125 and W175 (3.6−3.2 Å). At pH 5.2, *Xa*DHL is not active presumably because the side chain of H289 is present as the imidizolium ion; therefore, this structure of substrate bound to *Xa*DHL at low pH (*10*) is not likely an accurate representation of the ES-complex. Recent theoretical studies (*17*−*19*) show that in the ES-complex, the gauche-conformation of the substrate is bound with the leaving chlorine substituent hydrogen bonded only to W125 and not to W175. However, molecular dynamics simulations on the S_N2 transition-state show both the W125 and W175 are hydrogen-bonded to the leaving chlorine. Consistent with these theoretical studies, site-directed mutants W175Y and W175F are active but show a ∼10-fold lower specificity constant (k_{cat}/K_m), using 1,2-dibromoethane as a substrate (*4, 20*).

The *Rhodococcus* and *Xanthobacter* dehalogenases share considerable homology in the hydrolase core, but diverge significantly in the cap domain. While both enzymes are capable of catalyzing the hydrolysis of short-chain primary alkyl halides, the specificity of *Rr*DHL is much broader, encompassing longer chain linear, secondary, and cyclic alkyl halides (*4*). In addition, halides are uncompetitive product inhibitors of *Xa*DHL, while *Rr*DHL is not inhibited by halides at concentrations up to 80 mM. The lack of halide inhibition and broader substrate range suggests that the mechanism by which *Rr*DHL dehalogenates is different from that of *Xa*DHL. While the overall sequence of the two enzymes is quite similar, there are two significant differences in the active site residues. First, the *Rr*DHL (*2*) does not contain a tryptophan residue corresponding to W175 in *Xa*DHL (*21*). In addition, there is apparently no aspartate or glutamate corresponding to the triad residue D260 in *Xa*DHL. We report a 1.5 Å resolution crystal structure of a *Rhodococcus* dehalogenase. Structures were obtained at pH 5.5, pH 7.0 and pH 5.5 with iodide bound in the active site.

MATERIALS AND METHODS

Protein Production. A 882 base pair fragment containing the *Rhodococcus sp* dehalogenase gene was isolated by PCR and subcloned into the pTrcHis expression vector (Invitrogen), yielding a construct that contains a N-terminal His-tag and a C-terminal EXFLAG detection tag. After transformation into the *E. coli* strain DH10β, cultures in SOC media were shaken at 37 °C overnight. Protein expression was induced by the addition of 1 mM isopropyl-1-thio-β-D-galactopyranoside and induction was allowed to proceed for 5 h. The cells were then harvested by centrifugation and washed with 10 mM Tris-SO_4, 1 mM EDTA, pH 7.5. The cell pellets were stored at −70 °C prior to cell lysis. N-terminal His-tag and C-terminal EXFLAG increased the expression and stabilized the dehalogenase but were not used in the purification scheme.

Cells were thawed and suspended in 40 mL buffer A (10 mM Tris-SO_4, 1 mM EDTA, pH 7.5). Cells were disrupted by sonication. The resulting suspension was centrifuged at 19800*g* for 20 min. The cell free extract was fractionated using 45−70% saturated ammonium sulfate. The final pellet was suspended in buffer A then dialyzed overnight at 4 °C. This crude preparation was applied to a QAE column (Pharmacia) that had been equilibrated with buffer A. The dehalogenase bound to column and was eluted in buffer A containing 200 mM ammonium sulfate. Active fractions were pooled and concentrated by ultrafiltration to 25 mg/ml. The concentrated protein was applied to a Superdex 75 size exclusion column and eluted with buffer A containing 150 mM Na_2SO_4. Samples for crystallization were also chromatographed on a Sephadex G-75 size exclusion column (1.6 cm diameter × 200 cm) and eluted with buffer A containing 150 mM Na_2SO_4. Protein homogeneity was established by SDS-PAGE.

Site-Directed Mutagenesis. W118F and W118Y *Rr*DHL mutations were created using PCR-based point mutagenesis (*22*). The mutated dehalogenase genes were subcloned into the pET-3a vector. For overexpression of mutant dehalogenases, the pET-3a vector was transformed into competent *E. coli* BL21 (DE3). Clones were confirmed by DNA sequencing using the dideoxy-terminator cycle-sequencing method, using a Perkin-Elmer Model 310 DNA sequencer (Foster City, CA) (*23*).

Steady-State Kinetics. Enzyme activity was assayed using a pH-indicator dye system as described previously (*4*). Briefly, buffers were removed from enzyme solutions by

Table 1: Summary of Crystallographic Analysis

data set[a]	pH 5.5	pH 7.0	NaI	Native	AuKI	HgKI	NdAc	HgI_2	SmAc
source[b]	x8c	x8c	x8c	Home	Home	Home	Home	Home	Home
temperature (K)	100	100	100	293	293	293	293	293	293
resolution (Å)	1.5	1.5	1.5	2.5	2.5	2.5	2.5	2.5	2.5
unique reflections	52882	53599	47965	12318	10959	12196	11766	11946	11967
completeness (%)	97.8	97.2	93.1	99.1	88.2	98.1	94.7	96.1	96.3
(final shell)	(87.5)	(83.6)	(75.6)	(98.5)	(80.7)	(93.0)	(90.6)	(93.4)	(91.8)
multiplicity	3.4	4.8	4.6	5.7	3.5	6.8	7.1	4.5	5.7
R_{merge} (%)[c]	3.2	6.5	4.6	2.6	8.7	6.5	6.5	8.2	5.3
R_{iso} (%)[d]					23.9	23.6	31.2	30.9	12.1
number of sites					3	5	2	4	3
phasing power[e]					1.04	1.11	0.44	1.10	0.64
Refinement:									
reflections used (3σ)	51664	51094	46905						
$R_{working}$ (%)[f]	15.9	16.8	17.5						
R_{free} (%)[f]	17.9	17.5	18.7						
water molecules	369	329	394						
RMS Deviations:									
bond lengths (Å)	0.02	0.03	0.006						
bond angles (deg)	1.79	2.65	1.51						

[a] pH 5.5 are data from a native crystal; pH 7.0 are data from a native crystal soaked into pH 7.0; NaI are data from native protein co-crystallized with 2mM sodium iodide; AuKI = gold potassium iodide soak; HgKI = mercuric potassium iodide soak; NdAc = neodymium acetate soak; HgI_2 = mercuric iodide soak; SmAc = samarium acetate soak. [b] 'x8c' is beamline x8c, National Synchrotron Light Source, Brookhaven, NY. 'home' is a Rigaku RU200 rotating anode with CuKα radiation. [c] $R_{merge} = \sum|I_{obs} - \langle I\rangle|/\sum I_{obs}$, summed over all reflections. [d] $R_{iso} = \sum|F_{der} - F_{nat}|/\sum F_{nat}$, summed over all reflections. [e] Phasing power $= F_h/A$ where F_h is the heavy atom structure factor amplitude and A is the residual lack of closure. The overall figure of merit (FOM) for the 5 derivatives is 0.70. [f] 5% of the data were excluded from refinement and were used to determine the R_{free}. The $R_{working}$ does not include these reflections. In both cases $R=\sum(|F_{obs}| - k|F_{calc}|)/\sum|F_{obs}|$, with an appropriate choice of reflections for the summation.

dialysis against a solution containing 50 mM Na_2SO_4 and 1 mM EDTA, with the pH adjusted to 8.2, using 1 N H_2SO_4 or NaOH. Assays were carried out at pH 8.2, using 50 μM *m*-cresol purple (pK_a 8.3, λ_{max} 578 nm) as a pH indicator. Taps (pK_a 8.4) was added to the assay mixture to a concentration of 1 mM. Prior to each kinetic determination, the pH-indicator dye was titrated with a standardized solution of HCl to provide an apparent extinction coefficient. The steady-state kinetic constants for *Rr*DHL were determined at 25 °C. Kinetic constants were calculated from initial rates using the computer program HYPER (*24*).

Crystallization. Pure *Rhodococcus sp.* dehalogenase (~5 mg/ml) in 10 mM Tris-SO_4 buffer (pH 7.5), 1 mM EDTA, and 150 mM $(NH_4)_2SO_4$ was used to set up sparse matrix crystallization trials. The hanging drop technique was used, with 1 μL protein solution being mixed with 1 μL reservoir solution and suspended over 0.75 mL of reservoir solution. After 24 h at 8 °C, diffraction quality crystals were observed in a drop over a reservoir, containing 25% PEG 1.5K, 0.1M MES, pH 5.5, 0.3M sodium acetate. To produce crystals of sufficient size for data collection, microseeding was required to limit the number of nucleation sites. Crystals with a rectangular prism morphology grew to dimensions up to 0.15 mm × 0.15 mm × 0.5 mm. The crystals belonged to the space group $P2_12_12$ (space group #18), with cell dimensions a = 93.63 Å, b = 79.89 Å, c = 42.93 Å. The diffraction limit beyond 1 Å was observed on a large crystals that were flash frozen in a cryoprotectant consisting of 10% glycerol, 10% ethylene glycol, and 80% stabilizing solution (30% PEG 1.5K, 0.1M MES, pH 5.5, 0.2M sodium acetate). The dehalogenase was crystallized in the presence of NaI (2 mM) under similar conditions as the native crystals.

Data Collection/Structure Solution. Crystallographic data were obtained at beamline x8c at the National Synchrotron Light Source, Brookhaven National Laboratory. Beamline x8c is equipped with a 30 cm MAR (MAR Research, Hamburg Germany) imaging plate area detector (λ = 0.8157 Å, ~20 s exposure). Data to 1.5 Å resolution were collected on a cryoprotected-frozen crystal of the *Rhodococcus* dehalogenase at pH5.5 and on frozen cryoprotected crystals that had previously been soaked into pH 7.0 or pH 9.0 buffer (30% PEG 1.5K, 0.1M HEPES, pH 7.0, 0.2M sodium acetate or 30% PEG 1.5K, 0.1M CHES, pH 9.0, 0.2M sodium acetate). Finally, a data set was collected from a frozen cocrystals of dehalogenase and NaI, (λ = 1.072 Å). Data were processed using MOSFLM v5.0 and scaled using programs from the CCP4 package (*25*).

A native data set collected on a capillary mounted crystal at room temperature was used as the reference for heavy atom derivative searches and scaling. Screening solutions for heavy atom searches were prepared by placing a small amount of a heavy metal salt into the stabilizing solution and removing any insoluble salt with a microfuge. Then, a dehalogenase crystal was transferred into a 5 μL drop of the heavy atom screening solution and placed over a well of the stabilizing solution. Crystals thus treated were then back-soaked into stabilizing solution for at least 24 h before x-ray diffraction screening. Partial data sets were collected at room temperature and processed with DENZO (*26*). The automatic heavy atom solution/refinement program SOLVE (http://www.solve.lanl.gov) was used to choose potentially useful derivatives, to scale the derivative and native data, refine the positions of the heavy atoms, and provide the initial phasing (*27*). Five heavy atom derivatives were identified, and data from these derivatives are summarized in Table 1. After solvent flattening using the program DM in the CCP4 suite, the overall figure of merit (FOM), using these five derivatives, was 0.7.

Refinement. An initial model was built into the experimental map using the program O (*28*). This model contained

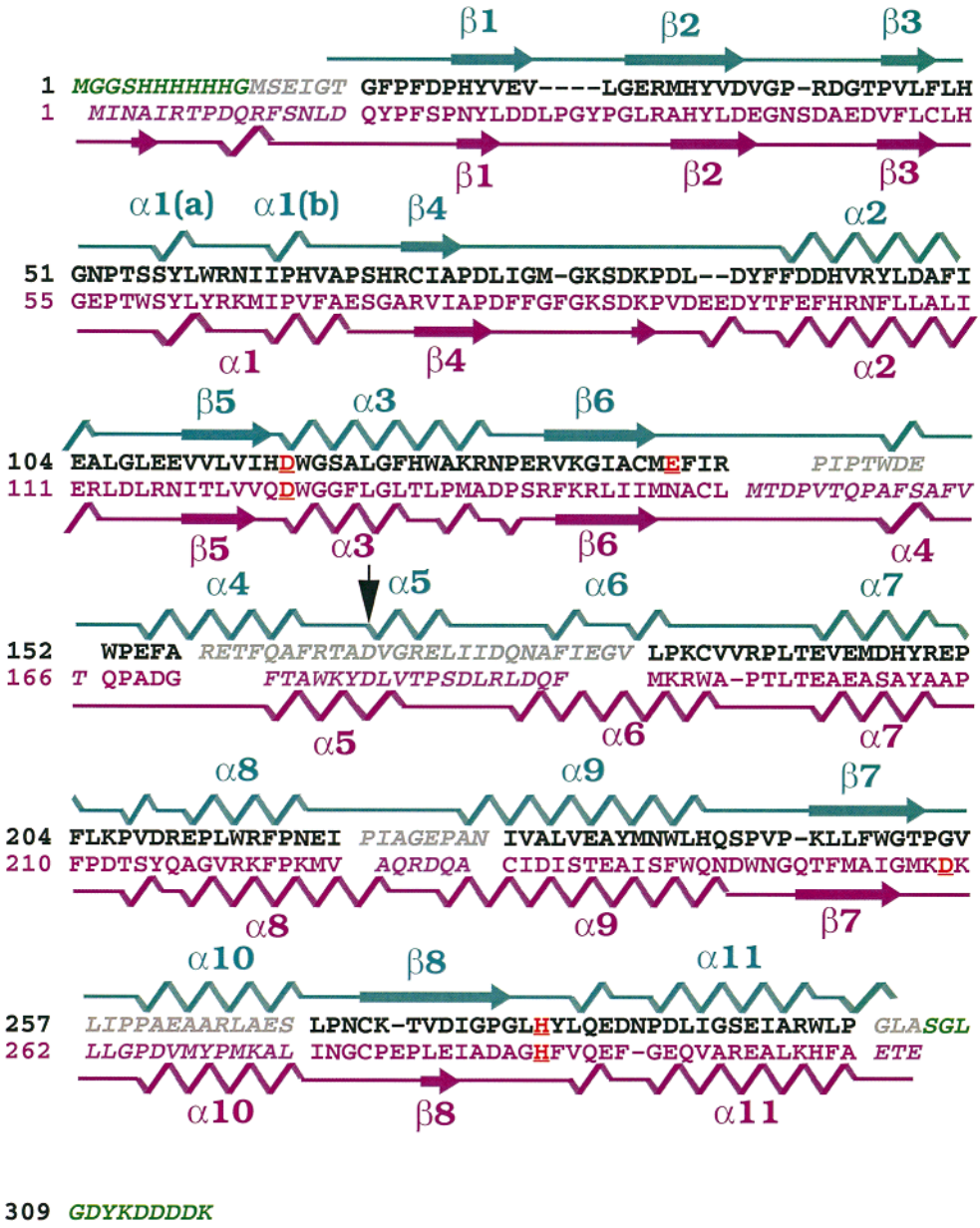

FIGURE 1: Structure-based sequence alignment of the *Rhodococcus* and *Xanthobacter* dehalogenases. The *Rhodococcus* sequence is in black/grey with the tags shown in green. The residues considered equivalent by superposition are printed in block letters. The *Xanthobacter* sequence is colored pink. The catalytic triad residues of both proteins are colored red and underlined. The black arrow marks aspartic acid residue D167, which lies in a region that is less ordered at pH 7.0. Secondary structure assignments are from PROCHECK (*48*). The superposition was obtained from O and the italicized sequence was not used in the structure alignment.

residues 15−304 (numbering starts from the beginning of the N-terminal tag). This model was used as a starting model for a slowcool refinement against the native (pH 5.5) 1.5 Å synchrotron data set using XPLOR (*29*). After slowcool and individual *B*-factor refinement, the *R*-value was 27.1%. We used the CNS package (*30*) for further refinement of this model, for a model of the dehalogenase at pH 7.0 and a model of the dehalogenase with iodide bound. In all cases, a maximum likelihood target was used. In the refinement of the iodide-bound structure, care was taken not to impose any expectation on the S−I distance. In this case, program default weighting scheme (WA) was used leading to the slight deviation from ideality in the bond lengths and angles of the NaI (Table 1). In all cases, refinement proceeded stepwise, with cycles of minimization, temperature factor, and occupancy refinement alternating with manual model building and water picking using O. Final refinement statistics are shown in Table 1.

RESULTS AND DISCUSSION

Structure of the Rhodococcus Dehalogenase. The structures of *Rhodococcus* dehalogenase at pH 5.5, pH 7.0, and a complex of the enzyme with bound iodide have been solved to 1.5 Å resolution. The *Xanthobacter* and *Rhodococcus* dehalogenases share a 30% amino acid sequence identity (Figure 1). Despite the structural similarity of the two enzymes, attempts to phase the *Rhodococcus* data using the structure of the *Xanthobacter* enzyme were unsuccessful. The structure of the *Rhodococcus* dehalogenase was solved by MIR, using five heavy atom derivatives. As in the *Xanthobacter* enzyme, heavy atoms were seen in the active site of the *Rhodococcus* structure (*31*). Crystallographic data are

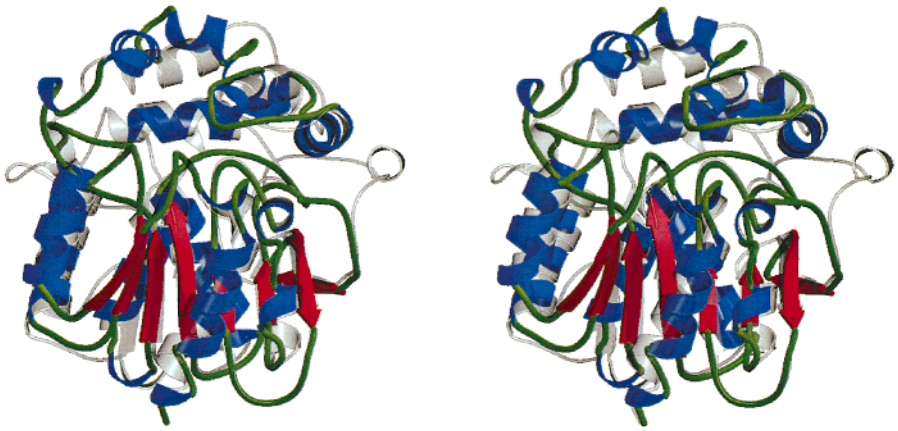

FIGURE 2: Stereo plot of the *Rhodococcus* dehalogenase prepared with the programs Molscript (*49*) and Raster3D (*50*). Helices are colored blue, strands red, with coil and turns colored green. Overlaid is the structure of the *Xanthobacter* enzyme. This superposition was generated in O, and gives an rmsd of 1.8 Å over 230 equivalent C^{α} positions.

summarized in Table 1. All the structures have $R_{working}$ of ~16%, (R_{free} ~18%) and show clear electron density from residue 15 (numbering starts at the N-terminal tag) to residue 305.

The overall structure of the *Rhodococcus* dehalogenase is very similar to that of the *Xanthobacter* dehalogenase; the root-mean-square deviation (rmsd) of over 230 equivalent C^{α} positions of the two enzymes is 1.8 Å. Both dehalogenase structures contain the defining α/β hydrolase core with a helical cap domain, which is found as an excursion between β6 and β7. This cap domain consists of six helices and forms a single layer of helix, which shields the catalytic triad, and creates the active site cavity (Figure 2).

α/β Hydrolase Fold. As discussed above, the haloalkane dehalogenases fall into the α/β hydrolase fold superfamily (*15*, *16*). Within this protein family, the core of the protein contains an eight-stranded β-sheet connected by α-helices. The sheet is primarily parallel, with a single strand, β2 adopting an antiparallel orientation. The enzymes of this class all contain a triad of catalytic residues. The positions of the triad residues are conserved relative to the secondary structure elements that make up the core of the α/β hydrolase fold. The primary nucleophile, aspartic acid in dehalogenases, is located at the nucleophilic elbow, a sharp turn between β5 and α3. The histidine is found on the loop joining β8 and the terminal helix. In the vast majority of cases, the third member of the triad, an acidic residue, is located on the loop between β7 and the penultimate helix (*15*).

The elements of secondary structure found in the core domain are well-conserved between the two dehalogenases; the cap domains show greater differences. This is consistent with the trend found more generally between the members of the α/β hydrolase superfamily: the core domain provides the catalytic residues the positions of which are well-conserved within the superfamily. Excursions from the core, including the dehalogenase cap domains, provide the substrate specificity and exhibit greater variation.

Cap Domain. The cap domains are regions where the two enzymes diverge significantly (Figure 2). In particular, helix α5 of the *Rhodococcus* cap domain is disrupted by a turn, giving two short helices almost at right angles to each other. This turn contains D167, which apart from D117 of the catalytic triad is the only residue to have φ and ψ angles that fall in an unfavorable region of the Ramachandran plot.

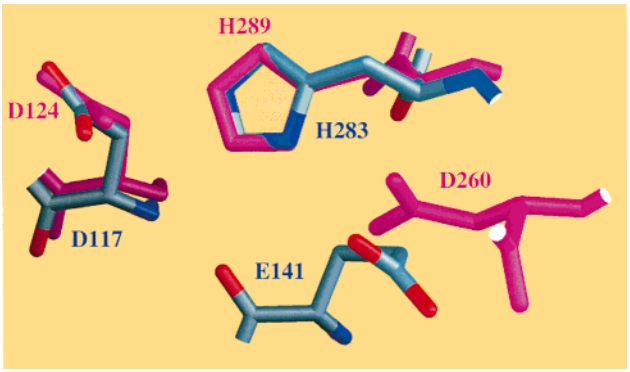

FIGURE 3: Overlay of the catalytic triad residues in the *Rhodococcus* and *Xanthobacter* (magenta) dehalogenases. The superposition was generated in O, using the atoms of the histidine and aspartic acid residues. The equivalent oxygen atom of the third residues are within 1 Å of each other. This figure was generated in GRASP (*51*).

Active Site. Another clear difference is the substitution in the *Rhodococcus* enzyme of a glutamic acid (E141) residue for the catalytic triad aspartic acid residue D260 in *Xa*DHL (Figure 3). The structure-based sequence alignment shows that in the *Rhodococcus* dehalogenase the equivalent position to D260 of *Xa*DHL is a glycine residue (Figure 1). As is obvious from sequence alignments, there is simply no suitable acidic residue that could substitute for D260 of *Xa*DHL in this region of the *Rhodococcus* enzyme. On the basis of the topology of the triad in lipases, Janssen and co-workers suggested that a glutamate or aspartate following strand β6 as the most likely alternate for this third member of the catalytic triad (*32*). Our structure confirms that the triad in the *Rhodococcus* dehalogenase consists of the nucleophilic D117, H283, and E141. The rmsd of the 18 equivalent atom positions (atoms of the nucleophilic aspartic acid residue and of the histidine residue) when overlaid is 0.4 Å (Figure 3).

The aspartate−histidine couple in the *Xanthobacter* enzyme is in the *syn*-conformation where the H289 $N^{\delta}H$ is apparently in a bifurcated hydrogen bond with both $O^{\delta 1}$ and $O^{\delta 2}$ of D260. The involvement of the *syn*-lone pair in the aspartate−histidine hydrogen bond is typical of most of the α/β hydrolases as well as the serine proteases (*33*). However, in the *Rhodococcus* enzyme, E141 is oriented so that the *anti*-lone pair on $O^{\epsilon 1}$ the carboxylate is apparently H-bonded

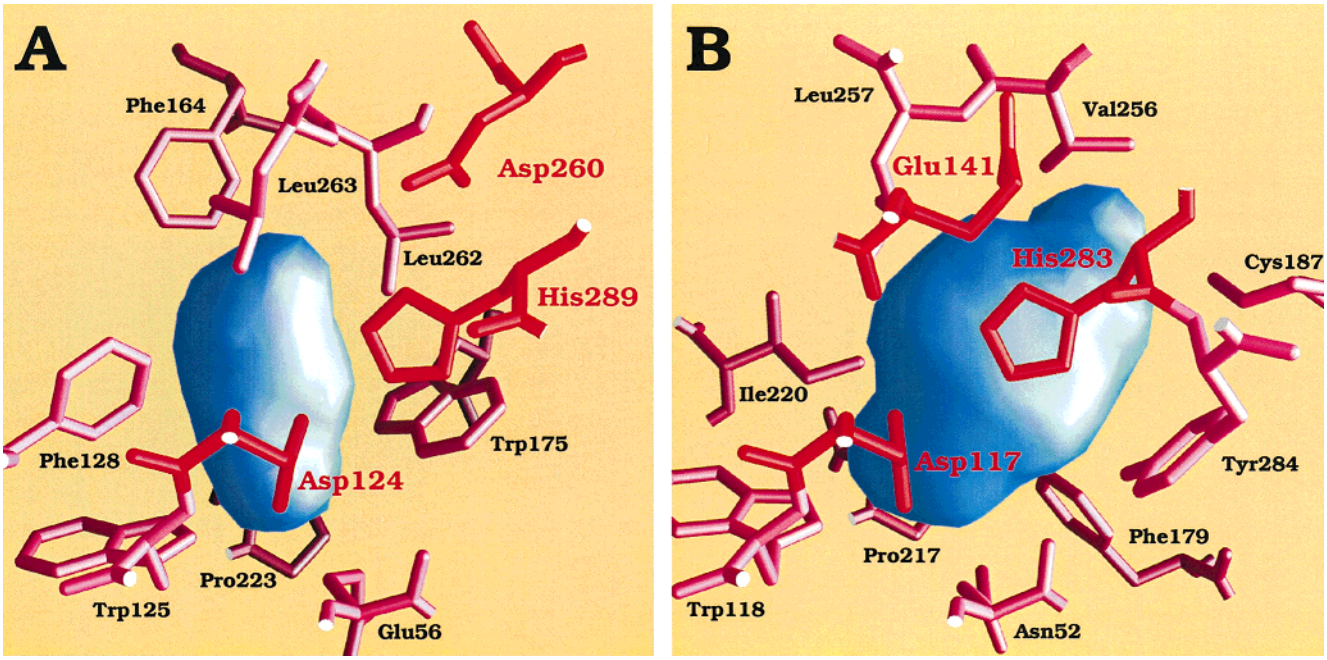

FIGURE 4: GRASP representation of the active site cavitites of the (A) *Xanthobacter* and (B) *Rhodococcus* dehalogenases. The residues of the catalytic triads are colored red, and residues which contribute atoms to the cavity/protein interface are colored pink. The *Rhodococcus* cavity encloses 187 Å^3, compared to the 96 Å^3 in the *Xanthobacter* active site. The *Rhodococcus* cavity has a decided bulge; this may allow additional orientations of the substrate, enabling this enzyme to remove both primary and secondary halide ions. The calculations of cavity volume were performed in GRASP (*51*).

to N$^{\delta}$H of H283 (Figure 3). The anti H-bond configuration is stabilized by apparent hydrogen bonds between O$^{\epsilon 2}$ of E141 and backbone NH's of V256 (3.0 Å) and I258 (3.0 Å). While the *anti*-configuration of the His−Asp/Glu couple is unusual, it has been observed. For example, the aspartic acid of the triad in horse pancreatic lipase (D176), is found in the same topology as E141 in the *Rr*DHL (*34*). Namely, in pancreatic lipase, D176 is located in the sequence just after β6 strand, its *anti*-lone pair is in a hydrogen bond with N$^{\delta}$H of H263, and the *anti*-configuration is stabilized by hydrogen bonds to backbone amides. Because of nature's strong preference for the syn Asp−His couple, it was originally proposed that *syn*-carboxylate could be 10^3-10^4 more basic then the *anti*-carboxylate (*35*). More recent studies with model compounds indicate that the *syn*-carboxylate is only a modestly stronger base then the *anti*-carboxylate (*33, 36, 37*).

Both enzymes have an active site cavity close to the catalytic triad. However, the *Rhodococcus* enzyme cavity is significantly larger, in both length and breadth, than in the *Xanthobacter* enzyme. In general, both active sites are lined with hydrophobic, primarily aromatic residues (Figure 4). The cluster of residues that define the *Rhodococcus* active site cavity include F179, F216, F124, I220, I115, P217, L257, and V256. The only polar residues in this cluster are tyrosine (Y284) and a cysteine residue (C187). As predicted from sequence alignments, one of two tryptophan residues (W175) present in the *Xanthobacter* active site is not conserved. The greater volume of the active site cavity in the *Rhodococcus* enzymes seems to be primarily due to the absence of this tryptophan residue. Although the enzyme was not cocrystallized with anything that would be an obvious substrate analogue, there is well-defined electron density at the active site of our model of the *Rhodococcus* dehalogenase (Figure 5b). This electron density can be readily modeled by an acetate ion.

pH Induced Changes. Except for very local changes in the linker region where the cap domain diverges from and rejoins the α/β hydrolase core of the protein, the structures of the *Rhodococcus* enzyme at pH 5.5 and pH 7.0 are essentially identical. Soaking the crystals in higher pH buffer affected the quality of the diffraction. The crystal at pH 7.0 showed higher mosaicity and diffracted X-rays less strongly. Nevertheless, the pH 7.0 soaked crystal diffracted to well beyond 1.5 Å. A crystal that had been soaked in pH 9.0 buffer was more severely effected; data from this crystal could not be processed, due in part to the crystals extremely high mosaicity.

Superimposing the pH 5.5 and pH 7.0 structures gives a rmsd on the C$^{\alpha}$ positions of 0.28 Å. A comparison of the waters of these two structures shows that the majority of them are found in both. The major difference between the pH 7.0 structure and that determined at pH 5.5 is that the region 164−168 is somewhat disordered in the pH 7.0 model. This region is not involved in crystal contacts, although the side chains of residues 165 and 168 are within 5 Å of the C-terminus of a symmetry related molecule. The density around residues 166−168 at pH 7.0 is continuous, but weak, and is best modeled by two conformations. There is no ambiguity in this region at pH 5.5; indeed, the Ramachandran outlier D167 is very well-defined in density (Figure 5a). The density for W152 is also extended in the pH 7.0 maps. This was modeled once again by two conformers, which share the same density for the six-membered ring, but flip the positions of the five-membered rings and the C$^{\beta}$ atom. The loosening of the structure in the cap domain at higher pH seems to propagate down into the linker region and is mediated by the side chain flip of W152. It is tempting to suggest that one of the effects of higher pH is to free up the

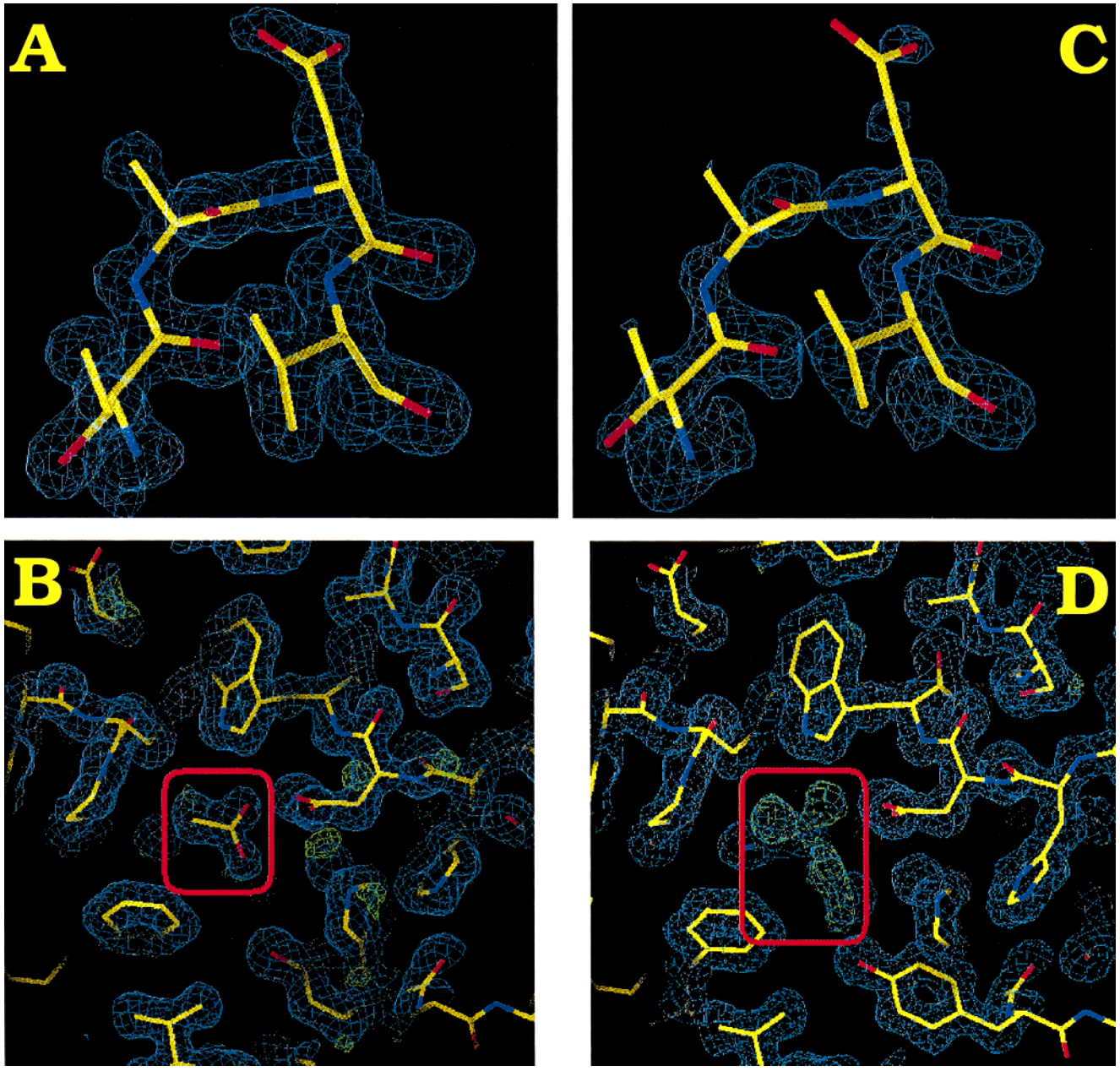

FIGURE 5: Structural differences in the *Rr*DHL at pH 5.5 (A, B) and pH 7.0 (C, D). Residues 164−168 form an extended elbow between helices α4 and α5 of the cap domain, and appear to become disordered at higher pH. (A) Residues 166−168 at pH 5.5, surrounded by electron density contoured at 1.4σ. (C) The same region at pH 7.0 with density contoured to 1.4σ. (B) The density found in the active site (outlined in red) was modeled convincingly by an acetate ion in the pH 5.5 structure. (D) While at pH 7.0, the density is significantly elongated, and can no longer be modeled by acetate ion alone. $2F_o - F_c$ density (at 1σ) is colored blue, and a $+3\sigma$ $F_o - F_c$ map is colored green. Nothing has been modeled into the density at the active site at pH 7.0. This figure was generated using the program O.

linker region, and perhaps allow access into the active site. This would imply that the pH profile of the enzyme is not strictly a function of the residues involved in catalysis but could also be a result of the relaxation in structure required to free up access to and egress from the active site. As discussed above, density is observed in the active sites of the enzyme at both pHs. At pH 5.5, the density was readily modeled by an acetate ion. However, at pH 7.0 the density is more extensive, and less convincingly described by acetate (Figure 5b).

Iodide Binding. While cocrystals of the *Rhodococcus* enzyme and sodium iodide (2 mM) were of higher mosaicity then native enzyme, they still diffracted to a nominal resolution of 1.5 Å. A difference Fourier map, using native phases, showed two large (>20σ) peaks in the area of the active site. These peaks were modeled as iodide ions, and the structure refined in CNS. On the basis of these models, the iodide sites had an occupancy of 59 and 53%. Clearly, this is too much electron density to be explained, for example, by sodium or oxygen atoms. Iodide binding did not cause gross changes in the protein structure. Minor changes in the structure include an increase in the number of active site waters, most of which interact with the iodide ions. In addition, iodide binding caused some movement of the side chain of D117, which with halide bound could be modeled with two conformations. However, the D117 side chain remained predominately in the conformation observed in the native protein model. Both iodines bind in the active site region but adopt quite different modes of binding. The first binds above the pyrrolidine ring of P217, interacting

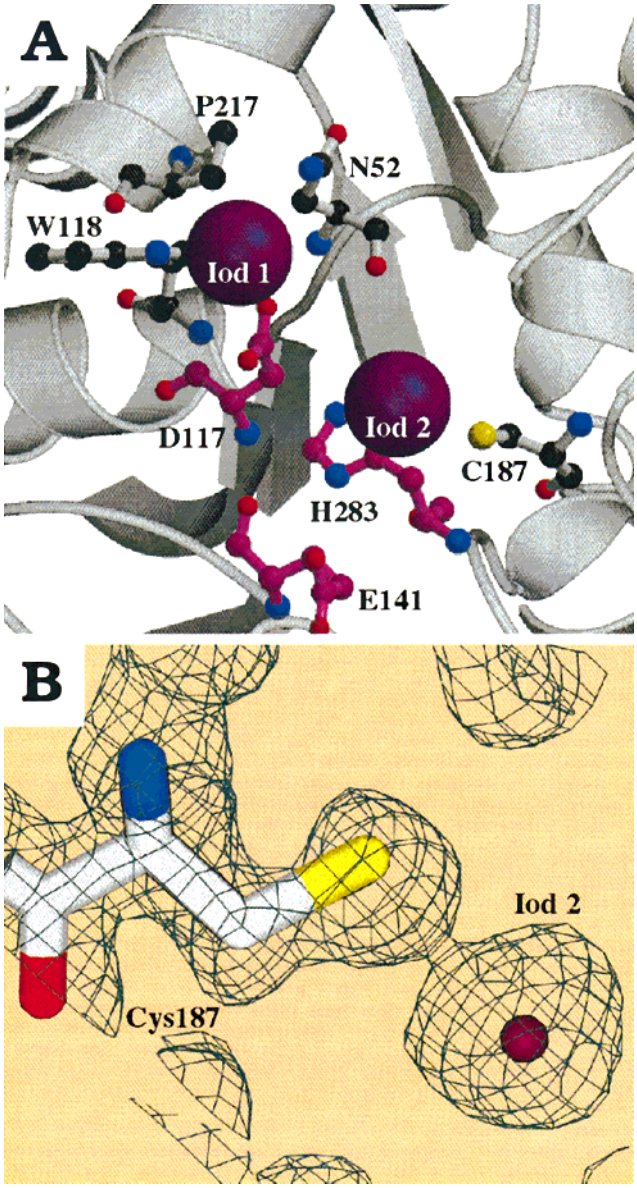

FIGURE 6: (A) Molscript/Raster3D representation of the iodide binding sites in the *Rhodococcus* dehalogenase. The iodines are shown as purple CPK spheres. The side chains of amino acid residues close the iodides are depicted. Also included are the catalytic triad residues (pink). We believe the iodide site labeled 'Iod1′ defines the normal halide-binding site. Three residues, P217, W118, and N52 surround Iod1, with Nϵ1 of W118 and Nδ2 of N52 within hydrogen-bonding distance (3.6−3.7 Å). The second iodine (Iod2) closely approaches the side chain of C187, and is ∼2.7 Å away from the sulfur of this residue. (B) Close-up of $2F_o - F_c$ density around the S−I bond. The density is contoured at 1.5σ; this diagram was produced using the program SPOCK (*52*).

with the NH's from W118 and N52; the second iodide sits very close (∼2.7 Å) to the S$^{\gamma}$ of C187 (Figure 6a).

Iodide Site 1. As products of the dehalogenase reaction, halides have been shown to bind to the *Xanthobacter* enzyme by interactions with two tryptophan residues, W125 and W175. *Xa*DHL crystallized in the presence chloride or iodide shows halide bound equidistant from the N$^{\eta}$ of W125 (3.4 Å) and N$^{\eta}$ of W175 (3.3 Å) (*10*). Because W125 in *Xa*DHL corresponds to W118 in the *Rhodococcus* sequence, the first iodide-binding site represents the product-binding pocket. Similar to *Xa*DHL, the iodide is within hydrogen bonding distance (3.5 Å) of N$^{\eta}$ of W118. As discussed above, the *Rhodococcus* enzyme does not have a tryptophan corresponding to W175 in *Xa*DHL. In the *Rhodococcus* structure, the iodide bound in site one is also stabilized by interaction with the N$^{\delta}$H on N52 (3.7 Å).

The binding of iodide in the active site of the *Rhodococcus* enzyme is somewhat at odds with our recent steady-state kinetic analysis (*4*). We showed that while iodide is an uncompetitive inhibitor of *Xa*DHL, it does not inhibit the enzyme from *Rhodococcus rhodochrous*. In the case of the *Xanthobacter* enzyme, halide binding is pH-dependent with the inhibition constant for chloride decreasing more then 20-fold from 61 mM at pH 8.9 to 2.9 mM at pH 6.5. Possibly the same type of pH-dependent behavior allows iodide to bind to the *Rhodococcus* enzyme at pH 5.5 in the crystal, but not at pH 7−9 where the enzyme activity is measured.

Iodide Site 2. According to the criterion used by the Cambridge Structural Database (CSB), any sulfur−iodine interaction of ≤2.82 Å is considered to be covalent. This number is derived from the sum of the atomic radii with a 0.4 Å tolerance factor (*38*). Clearly, the S−I interaction has not been observed frequently enough to be confident in the covalent bond distance (*39*). However, in two CSB structures, triphenylmethyliodosulfane (*40*) and bis(thiourea)iodide(I) iodide (*41*), an S−I interatomic distance of ∼2.65 Å was observed consistent with a covalent bond. Even given iodine's extreme polarizability, the iodine in the second site is too close to the sulfur on the side chain of C187 (2.7 Å) to result from simple association. The sum of the nonbonded contact radii of iodine and sulfur would yield an expected interatomic distance of ∼3.8 Å (*42*). Along with short interatomic distance, the anisotropic distribution of electron density around the iodine suggests that its movement is coupled to the torsional freedom of the cysteine side chain (data not shown). Given these data, it appears that the interaction of the iodine with the active site cysteine residue is covalent (Figure 6b). The presence of a stable covalent S−I bond on C187 is puzzling. A reaction of a cysteine thiol or thiolate with iodide is not possible. We propose that in our NaI solution some I_2 formed by oxidation. In the presence of iodide, I_2 is readily converted to I_3^-, which is known to iodinate cysteine thiols (*43*). The most unusual feature of this iodinated cysteine is that it is stable. Iodinated cysteine residues react readily with other nucleophiles. For example, reaction of R−S−I with a second thiol would yield a disulfide. In addition, water is known to act as a nucleophile and decompose iodinated thiols to yield sulfenic acids. The stability of the C187 S−I bond implies that water cannot position itself in the active site of the protein to displace iodide. Interestingly, iodine is reported to inactivate a *Rhodococcus*-like dehalogenase from an *Acinetobacter* strain GJ70 (*44*). Iodination of a cysteine residue near the active site (C187 in *Rr*DHL) could be the mechanism by which iodine inactivates *Rhodococcus*-like dehalogenases.

Site-Directed Mutant W118F of RrDHL. To confirm that W118 was required for dehalogenase activity we prepared site directed mutants W118F and W118Y of *Rr*DHL. Table 2 compares the activities of W118F against primary, secondary, and cyclic alkylhalide substrates with that of wild-type *Rr*DHL. Substitution of phenylalanine for tryptophan at position 118 of the *Rhodococcus* enzyme results in significant increases in K_m and decreases in k_{cat} for all substrates. Similar effects on the K_m and k_{cat} were observed using the W118Y

Table 2: Steady State Kinetic Constants of *Rr*DHL

	Wildtype *Rr*DHL[a]			W118F *Rr*DHL[b]		
substrate	K_m (mM)	k_{cat} (s^{-1})	k_{cat}/K_m ($M^{-1}\ s^{-1}$)	K_m (mM)	k_{cat} (s^{-1})	k_{cat}/K_m ($M^{-1}\ s^{-1}$)
1,2-dibromoethane	1.2	6.2	5.2×10^3	2.2	0.91	4.1×10^2
1-bromobutane	0.35	0.98	2.8×10^3	1.6	0.12	7.5×10^1
1-chlorobutane	0.40	0.86	2.1×10^3	3.7	0.42	1.1×10^2
2-bromobutane	0.84	0.39	4.6×10^2	6.8	0.11	1.6×10^1
2-chlorobutane	9.4	0.32	2.7×10^2	$\gg 60$	0.021	
cyclopentylbromide	≤ 0.05	0.22	4.4×10^3	1.8	0.17	9.4×10^1

[a] Data reported in Schindler et al. (*4*). [b] Kinetic constants were determined using the proton release assay as described under Materials and Methods. The K_m values had errors of $\leq 20\%$. The k_{cat} values had errors of $\leq 8\%$.

mutant. The combined effect of changes of K_m and k_{cat} result in an approximately 10−50-fold decrease in the specificity constants (k_{cat}/K_m) for all substrates consistent with W118 being involved in substrate binding and activation.

Evolution of Dehalogenases. Database searches reveal significant homology between the *Xanthobacter* and *Rhodococcus* dehalogenases and many of the epoxide hydrolases (data not shown). We have used an alignment of 272 α/β hydrolase sequences from the PFAM database (*45*) as the starting point for phylogenetic analysis. While this analysis will be reported in detail elsewhere, it shows that the α/β hydrolase superfamily can be subdivided into four major groups: the peptidases, the lipases, the epoxide hydrolases, and the lactone hydrolases. The *Xanthobacter* and *Rhodococcus* dehalogenases are clustered tightly together on a subnode within the epoxide hydrolase branch of the α/β hydrolases. Despite the differences in their active site topology, this analysis suggests the *Xanthobacter* and the *Rhodococcus* dehalogenases arose from a common progenitor.

CONCLUSIONS

Haloalkane dehalogenases are potentially important biocatalysts with both industrial and bioremediation applications. Two classes of dehalogenases have been reported from *Xanthobacter* and *Rhodococcus*, which share 30% amino acid sequence identity. Phylogenetic analysis infers that these dehalogenases are closely related and fall with in the epoxide hydrolase node of the α/β hydrolase superfamily. While the *Xanthobacter* and *Rhodococcus* are similar in sequence, they have significantly different substrate specificity and halide-binding properties. We report the 1.5 Å resolution crystal structure of the *Rhodococcus* dehalogenase at pH 5.5, pH 7.0, and pH 5.5 in the presence of NaI, providing an opportunity for a detailed structural comparison of the enzymes. The enzymes show significant structural homology in the α/β hydrolase core but diverge considerably in the cap domain. The cap domains partially define the dehalogenase active site cavity and provide the structural basis for the significant differences in substrate specificity. Consistent with its broad specificity for primary, secondary, and cyclic haloalkanes, the *Rhodococcus* enzyme's active site cavity (187 $Å^3$) has almost twice the volume of the *Xanthobacter* enzyme active site (96 $Å^3$), which uses only short chain primary alkylhalides as substrates.

Significantly, the *Rhodococcus* dehalogenase has a different catalytic triad topology than the *Xanthobacter* enzyme. Both the identity and the position of nucleophilic aspartate and the histidine residues are conserved in the two enzymes. In *Xa*DHL, the carboxylate functionality of the triad is provided by D260, which is positioned on the loop between $\beta 7$ and the penultimate helix and is oriented so that its *syn*-lone pairs can hydrogen bond to $N^{\delta}H$ of H289. This topology is found in most α/β hydrolases. The carboxylate functionality in the *Rhodococcus* catalytic triad is donated from E141 located in the region following the $\beta 6$ strand. In contrast with the *Xanthobacter* enzyme, the *anti*-lone pair on $O^{\epsilon 1}$ of E141 in the *Rhodococcus* enzyme is positioned to H-bond $N^{\delta}H$ of H283. This triad topology has been observed in some members of the α/β hydrolase superfamily, including pancreatic lipase (*46*). Interestingly, a recent structure of the epoxide hydrolase from *Agrobacterium* demonstrated two aspartic acid residues one at each of the positions analogous to D260 in *Xa*DHL and E141 *Rr*DHL (*47*).

In both dehalogenases, a tryptophan residue follows the nucleophilic aspartate in the primary sequence. The indole $N^{\eta}H$ of W125 in *Xanthobacter* and W118 *Rhodococcus* are involved in substrate and product binding. In the *Xanthobacter* enzyme, bound substrate or halide product are also stabilized by interaction with the indole $N^{\eta}H$ of W175. While the *Rhodococcus* enzyme has no tryptophan analogous to W175, it stabilizes the bound halide with a hydrogen bond to $N^{\delta}H$ of N52. Finally, the differences in *Rhodococcus* structure at pH 5.5 and 7.0 may give clues about the conformational fluctuations required by this very compact protein to allow substrate access to and product egress from the active site.

ACKNOWLEDGMENT

We would like to thank the staff of beamline x8c at NSLS BNL for help during data collection. Thanks also to Peter Kenny, Tomas Lundqvist, Anthony Nicholls, and Roger Sayle for stimulating discussions.

REFERENCES

1. Janssen, D. B., Scheper, A., Dijkhuizen, L., and Witholt, B. (1985) *Appl. Environ. Microbiol. 49*, 673−7.
2. Kulakova, A. N., Stafford, T. M., Larkin, M. J., and Kulakov, L. A. (1995) *Plasmid 33*, 208−17.
3. Curragh, H., Flynn, O., Larkin, M. J., Stafford, T. M., Hamilton, J. T. G., and Harper, D. B. (1994) *Microbiology (Reading, U. K.) 140*, 1433−42.
4. Schindler, J. F., Naranjo, P. A., Honaberger, D. A., Chang, C.-H., Brainard, J. R., Vanderberg, L. A., and Unkefer, C. J. (1999) *Biochemistry 38*, 5772−5778.
5. Damborsky, J., Nyandoroh, D. G., Nemec, M., Holoubek, I., Bull, T., and Hardman, D. J. (1997) *Biotechnol. Appl. Biochem. 26*, 19−25.
6. Dolfing, J., van den Wijngaard, A. J., and Janssen, D. B. (1994) *Biodegradation 4*, 261−82.
7. Janssen, D. B., and Witholt, B. (1985) *Sci. Total Environ. 47*, 121−35.
8. Stucki, G., and Thuer, M. (1994) *Appl. Microbiol. Biotechnol. 42*, 167−72.
9. Verschueren, K. H., Franken, S. M., Rozeboom, H. J., Kalk, K. H., and Dijkstra, B. W. (1993) *J. Mol. Biol. 232*, 856−72.
10. Verschueren, K. H. G., Seljee, F., Rozeboom, H. J., Kalk, K. H., and Dijkstra, B. W. (1993) *Nature 363*, 693−8.
11. Pries, F., Kingma, J., Krooshof, G. H., Jeronimus-Stratingh, C. M., Bruins, A. P., and Janssen, D. B. (1995) *J. Biol. Chem. 270*, 10405−11.
12. Pries, F., Kingma, J., Pentenga, M., van Pouderoyen, G., Jeronimus-Stratingh, C. M., Bruins, A. P., and Janssen, D. B. (1994) *Biochemistry 33*, 1242−7.

13. Schanstra, J. P., and Janssen, D. B. (1996) *Biochemistry 35*, 5624−32.
14. Schanstra, J. P., Kingma, J., and Janssen, D. B. (1996) *J. Biol. Chem. 271*, 14747−14753.
15. Ollis, D. L., Cheah, E., Cygler, M., Dijkstra, B., Frolow, F., Franken, S. M., Harel, M., Remington, S. J., Silman, I., Schrag, J., Sussman, J. L., Verschueren, K. H. G., and Goldman, A. (1992) *Protein Engin. 5*, 197−211.
16. Heikinheimo, P., Goldman, A., Jeffries, C., and Ollis, D. L. (1999) *Structure 7*, R141−R146.
17. Lightstone, F. C., Zheng, Y.-J., Maulitz, A. H., and Bruice, T. C. (1997) *Proc. Natl. Acad. Sci. U.S.A. 94*, 8417−8420.
18. Lightstone, F. C., Zheng, Y.-J., and Bruice, T. C. (1998) *J. Am. Chem. Soc. 120*, 5611−5621.
19. Lightstone, F. C., Zheng, Y.-J., and Bruice, T. C. (1998) *Bioorg. Chem. 26*, 169−174.
20. Krooshof, G. H., Ridder, I. S., Tepper, A. W. J. W., Vos, G. J., Rozeboom, H. J., Kalk, K. H., Dijkstra, B. W., and Janssen, D. B. (1998) *Biochemistry 37*, 15013−15023.
21. Janssen, D. B., Pries, F., van der Ploeg, J., Kazemier, B., Terpstra, P., and Witholt, B. (1989) *J. Bacteriol. 171*, 6791−9.
22. Zhao, L. J., Zhang, Q. X., and Padmanabhan, R. (1993) *Methods Enzymol. 217*, 218−27.
23. Sanger, F., Nicklen, S., and Coulsen., A. R. (1977) *Proc. Natl. Acad. Sci. U.S.A. 74*, 5463−5467.
24. Cleland, W. W. (1979) *Methods Enzymol. 63*, 103−38.
25. Bailey, S. (1994) *Acta Crystallogr., Sect. D: Biol. Crystallogr. 50*, 760−763.
26. Otwinowski, Z., and Minor, W. (1997) *Methods Enzymol. 276*, 307−326.
27. Terwilliger, T. C., and Berendzen, J. (1999) *Acta Crystallogr., Sect. D: Biol. Crystallogr. D55*, 849−861.
28. Jones, T. A., Zou, J. Y., Cowan, S. W., and Kjeldgaard, M. (1991) *Acta Crystallogr., Sect. A: Found. Crystallogr. A47*, 110−19.
29. Brunger, A. T. (1992) *X-PLOR Version 3.1: A system for X-ray crystallography and NMR*, Yale University Press, New Haven, CT.
30. Brunger, A. T., Adams, P. D., Clore, G. M., DeLano, W. L., Gros, P., Grosse-Kunstleve, R. W., Jiang, J.-S., Kuszewski, J., Nilges, M., Pannu, N. S., Read, R. J., Rice, L. M., Simonson, T., and Warren, G. L. (1998) *Acta Crystallogr., Sect. D: Biol. Crystallogr. 54*, 905−921.
31. Verschueren, K. H., Franken, S. M., Rozeboom, H. J., Kalk, K. H., and Dijkstra, B. W. (1993) *FEBS Lett. 323*, 267−70.
32. Krooshof, G. H., Kwant, E. M., Damborsky, J., Koca, J., and Janssen, D. B. (1997) *Biochemistry 36*, 9571−9580.
33. Cramer, K. D., and Zimmerman, S. C. (1990) *J. Am. Chem. Soc. 112*, 3680−3682.
34. Bourne, Y., Martinez, C., Kerfelec, B., Lombardo, D., Chapus, C., and Cambillau, C. (1994) *J. Mol. Biol. 238*, 709−732.
35. Gandour, R. D. (1981) *Bioorg. Chem. 10*.
36. Zimmerman, S. C., and Cramer, K. D. (1988) *J. Am. Chem. Soc. 110*, 5906−5908.
37. Huff, J. B., Askew, B., Duff, R. J., and Rebek, J., Jr. (1988) *J. Am. Chem. Soc. 110*, xxxx.
38. CCDC. (1998), Cambridge Structural Database.
39. Allen, F. H., Kennard, O., Watson, D. G., Brammer, L., Orpen, A. G., and Taylor, R. (1987) *J. Chem. Soc., Perkin Trans 2*, S1−S19.
40. Minkwitz, R., Preut, H., and Sawatzki, J. (1988) *Z. Naturforsch., B: Chem. Sci. 43*, 399−402.
41. Lin, G., Hung-Yin, and Hope, H. (1972) *Acta Crystallogr. B28*, 643−646.
42. Rowland, R. S., and Taylor, R. (1996) *J. Phys. Chem. 100*, 7384−7391.
43. Cuatrecasas, P., and Hollenberg, M. D. (1976) in *Advances in Protein Chemistry* (Anfinsen, C. B., Edsall, J. T., and Richards, F. M., Eds.) pp 286−287, Academic Press, New York.
44. Janssen, D. B., Gerritse, J., Brackman, J., Kalk, C., Jager, D., and Witholt, B. (1988) *Eur. J. Biochem. 171*, 67−72.
45. Bateman, A., Birney, E., Durbin, R., Eddy, S. R., Finn, R. D., and Sonnhammer, E. L. L. (1999) *Nucleic Acids Res. 27*, 260−262.
46. Scharg, J. D., Winkler, F. K., and Cygler, M. (1992) *J. Biol. Chem. 267*, 4300−4303.
47. Nardini, M., Ridder, I. S., Rozenboom, H. J., Kalk, K. H., Rink, R., Janssen, D. B., and Dijkstra, B. W. (1999) *J. Biol. Chem. 274*, 14579−14586.
48. Laskowski, R. A., Macarthur, M. W., Moss, D. S., and Thornton, J. M. (1993) *J. Appl. Crystall. 26*, 283−291.
49. Kraulis, P. J. (1991) *J. Appl. Crystall. 24*, 946−950.
50. Merritt, E. A., and Bacon, D. J. (1997) *Methods Enzymol. 277*, 505−524.
51. Nicholls, A., Bharadwaj, R., and Honig, B. (1993) *Biophys. J. 64*, A166-A166.
52. Christopher, J. A. (1997), http://quorum.tamu.edu/jon/spock.

BI9913855